Iptycene-Assisted Alignment of Chirality-Sorted SWCNTs for Field-Effect Transistors

Monika R. Snowdon,[1,2] Ekaterina V. Sukhanova,[3] Zakhar I. Popov,[3] Shisheng Li,[2] Leanddas Nurdiwijayanto,[2] Takaaki Taniguchi,[2] Shinsuke Ishihara,[2] Takeshi Tanaka,[4] Hiromichi Kataura,[4] Kazuhito Tsukagoshi,[2] Robert L. F. Liang,[1,5] Marina Freire-Gormaly,[5] Derek J. Schipper[1*], Dmitry G. Kvashnin[3*] and Dai-Ming Tang[2,6*]

[1] Waterloo Institute for Nanotechnology, University of Waterloo, Waterloo, Ontario, N2L 3G1, Canada

[2] Research Center for Materials Nanoarchitectonics (MANA), National Institute for Materials Science (NIMS), Tsukuba 305-0044, Japan

[3] Emanuel Institute of Biochemical Physics of RAS, 4 Kosygin Street, Moscow 119334, Russian Federation

[4] Nanomaterials Research Institute, National Institute of Advanced Industrial Science and Technology (AIST), Tsukuba, Ibaraki 305-8565, Japan

[5] Lassonde School of Engineering, York University, North York, Ontario, M3J 2S5, Canada

[6] Institute of Pure and Applied Sciences, University of Tsukuba, Tsukuba, 305-8571 Japan

*Authors to whom correspondence should be addressed:

*Dai-Ming Tang, tang.daiming@nims.go.jp

*Derek J. Schipper, dschipper@uwaterloo.ca

*Dmitry G. Kvashnin, dgkvashnin@gmail.com

Abstract

Single-walled carbon nanotubes (SWCNTs) are ideal channel materials candidates for energy-efficient nanoscale transistors; however, it is challenging to achieve uniform alignment of semiconducting SWCNTs with homogeneous chirality. Here, we report the proof-of-concept of using organized chirality-sorted SWCNTs via the alignment relay technique (ART), where iptycene molecules order the nanotubes through π-π interactions. Top gated field-effect transistors (FETs) were fabricated with aligned (10,3) chirality SWCNTs as channels to show an I_{ON} of 3.8 μA, an I_{ON}/I_{OFF} ratio of 2.9×10^6, and a carrier mobility of 10.08 cm^2/Vs, which is enhanced by two magnitudes of order compared with a bundled SWCNTs network channel. In addition, ART was applied to align commercially available semiconducting SWCNTs to fabricate a chemiresistive gas sensor that showed prompt detection of 4 ppm ammonia (NH_3) with a sensitivity of 0.43 ± 0.04 %/ppm, demonstrating a general approach to align SWCNTs for applications in electronic devices.

Keywords: carbon nanotubes, chirality, transistors, sensors, iptycene, alignment, Ab initio calculations

Introduction

Single-walled carbon nanotubes (SWCNTs) are candidates as semiconducting (sc) channel materials for field-effect transistors (FETs) in the post-silicon era because of their quasi-one dimensional tubular structure, nanoscale thickness and high carrier mobility.[1] However, there are still challenges regarding uniformity in the nanotube structure and alignment. Fundamentally, the engineering of carbon nanotube chirality is crucial for their electronic applications.[2] Nanotubes with homogeneous chirality and therefore uniform electrical properties need to be separated to enhance the gating efficiency and reduce device-to-device variation. Furthermore, multiple nanotubes need to be aligned between the source and drain electrodes to achieve a high current.[3]

Recent advancements have been made in the separation of SWCNTs by centrifugation, extractions via polymers, small molecules, or aqueous two-phase separation, dielectrophoresis and gel chromatography.[4-12] For example, the gel chromatography method has allowed for large scale separation of semiconducting and even single-chirality SWCNTs.[6, 13] A combination of hydrogels and different surfactant-wrapped CNTs can extract sc-SWCNTs of specific chirality and handedness.[14, 15] Another approach of density gradient ultracentrifugation (DGU) is based on the density difference of CNTs with different diameters,[16] leading to pure SWCNT of uniform conductance and even enantiomers.[4] Dielectrophoresis (DEP) has also been developed for separating and depositing specific metallicities of SWCNTs. After the report by Krupke et al.,[12] the DEP production was subsequently upscaled.[15] Using DEP, researchers have fabricated CNTFETs based on aligned CNT semiconducting networks.[14]

After separation, alignment methods have been developed to assemble SWCNTs, either during or after their growth.[17] A nitrogen blowing method has yielded moderate alignment of the semiconducting SWCNTs.[18] Acid-functionalized SWCNTs have been shown to adsorb slightly

basic hafnia (HfO_2) surfaces selectively.[19] Alternatively, work by Sharma and Strano showed that an alternating pattern of polar and non-polar self-assembled monolayers on an Au surface can result in a highly aligned SWCNTs monolayer.[20] The process was possible due to droplets formed from a SWCNTs thin film placed on the functionalized surface. The droplets selectively migrated to areas with polar parallel patterns.[20] Numerous other examples of highly-dense arrays of CNTs for high-performance FETs have been extensively reviewed.[21] Up to now, there is limited work on the alignment of chirality-pure SWCNTs for transistor applications. By using a network of chirality-sorted (10,3) SWCNTs, transparent flexible thin film transistors have shown an on-current of ~50 nA, with a carrier mobility of 0.8 cm^2/Vs and a subthreshold swing (SS) of 2.3 V/dec.[22] To further enhance the transistor performance, improvements are needed on the device configuration, nanotube surface chemistry and alignment.

In this work, we explore a molecular approach for aligning chirality-sorted carbon nanotube to fabricate CNTFETs by using the alignment relay technique (ART) with iptycene molecular tweezers. In principle, the ART allows for alignment of nanotubes as well as sorting by length and diameter. The method is operationally simple, free of metal contaminants, and can be carried out without specialized equipment.[23, 24] As the proof-of-concept, we demonstrate that CNTFETs with aligned CNT channels could be fabricated by using the ART method. Chirality-sorted SWCNTs were assembled through a monolayer of aromatic tweezer molecules, leveraging the aligning properties of liquid crystals. Enhanced ON-current and carrier mobility was achieved with iptycene-aligned chirality-sorted SWCNTs, compared to bundled network channels. This work demonstrates the potential of applying ART to fabricate CNTFETs, marking a step forward in the development of high-performance electronic devices via molecular assembly. Additionally,

investigating ART can yield valuable insights into the fundamental nanoscopic dynamics of carbon nanotube behavior, liquid crystal interactions, and surface chemistry.

Results and discussion

SWCNT alignment

(10,3) SWCNTs were sourced from work by Kataura et al. through gel chromatography[25] with possible residual species of (7,6), (10,2), (6,5) and (8,3). Subsequently, aligned SWCNTs were produced with ART using the phosphonate ester iptycene molecules (**Figure 1a**).[26] A UV-ozone cleaned silicon (Si/SiO_2, SiO_2 = 200 nm) wad dipped into a newly prepared solution of the iptycene dissolved in nematic liquid crystal 4-Cyano-4'-pentylbiphenyl (5CB) and left to functionalize for 24 hours. The contact angle for a silicon wafer cleaned with UV-ozone (30 mins) was 12.1±3.7°, which became 36.8±1.4° with an iptycene monolayer.

The iptycene-aligned substrate was then exposed to a solution of (10,3) SWCNTs in a humid environment and then characterized for alignment by atomic force microscopy (AFM) and scanning electron microscopy (SEM). On average, the nanotubes were 1 µm in length and ~61.9% were aligned (±10°), with a density of 0.35 SWCNTs/μm^2 as per SEM micrograph in **Figure 1b**. Additional details for the alignment calculations are available in the Supporting Information (SI, **Figure S1**).

Device fabrication

We fabricated transistors in bottom-gated (BG) and top-gated (TG) configurations, as shown in Schematics in **Figure 1a** and **1c**. Top-gated devices had a 20 nm Al_2O_3 dielectric layer, whereas bottom-gated ones had 200 nm of SiO_2. The conditions for metal deposition are shown in **Table S1** (SI). The bottom-gated device used for gas sensor testing had ART aligned sc-SWCNTs of

90% purity from Nanointegris, Inc (Canada).[27] As from our previous work, the density of tubes on the surface is 0.3 ±0.05 CNTs/μm^2.[28] There appears to be a trade-off between alignment and packing density, as evidenced by experiments showing improved alignment but decreased density with sonication treatment.[27]

FET performance

We compared the nanotube transistor performance of aligned arrays and bundled networks. A top-gated aligned CNT transistor is shown in **Figure 2a**, along with the corresponding output plot (**Figure 2b**). The aligned and bundled network (10,3) SWCNT devices are compared as both the linear (**Figure 2c**) and log-plot (**Figure 2d**). Optimal results were achieved after annealing at 300°C for 3h and whilst the device was under vacuum.

Devices were tested in both the TG and BG configuration, and the TG device showed superior results. The FET with tube bundles had an I_{ON} of 0.02 μA, an I_{ON}/I_{OFF} of 2.1×10^5 and a mobility of 1.3×10^{-2} cm^2/Vs at V_{SD} = 1 V. The FET with aligned SWCNTs demonstrated an I_{ON} of 3.83 μA, an I_{ON}/I_{OFF} of 2.9×10^6, a mobility of 10.08 cm^2/Vs, and a subthreshold swing (SS) of 0.45 V/dec. The aligned device had a high I_{ON} value, nearly 200 times higher than the bundled tubes, and the I_{ON}/I_{OFF} ratio of the aligned tubes were one order of magnitude higher (10^6 vs 10^5). Additional data and micrographs pertaining to the bundled device with (10,3) SWCNTs are available in the SI, **Figure S2**. These experimental results demonstrate that the aligned SWCNTs have a higher carrier mobility, on the order of two magnitudes higher than bundled SWCNTs do. This difference is attributed to the scattering of electrons and resistance by the crossed CNTs in the bundled network. Compared with the reported state-of-art CNTFETs, the performance of our devices is limited to the low packing density. On the other hand, the low density allows us to compare the transport

properties of intrinsic and crossed CNT building blocks, and our data indicate that CNT crossings could increase the resistance by 200 times.

Then, performance of the FETs under vacuum and air were compared (**Figure 3**). The performance of our bundled CNT network-based device is comparable with the thin-film transistor device that used the same single-chirality (10,3) SWCNTs,[22] while the aligned nanotube devices demonstrated superior transport properties. Top gated devices obtained an average I_{ON}/I_{OFF} of 10^6 in air and in vacuum for the aligned devices, yet the bundle devices peaked at 10^5 (**Figure 3a**). In addition, the carrier mobility of the TG aligned devices was higher in both environmental conditions by 100x compared to the bundled network. The overall performance was higher in terms of carrier mobility and I_{ON}/I_{OFF} ratio for the top-gated aligned device in vacuum. However, when the same device was tested under ambient air conditions the I_{ON} value increased from 3.8 μA to 4.9 μA as shown in **Figure 3**, probably due to doping effects from oxygen in air.[29]

When comparing the same device tested as both a top-gate (TG) and bottom-gate (BG) transistor, the TG configuration outperforms its BG counterpart in terms of the I_{ON}/I_{OFF} value (10^6 in the top-gate versus 10^5 in the bottom-gate; **Table S2**). On the other hand, the BG equivalent tested under vacuum demonstrates only a slightly lower carrier mobility of 9.2 cm^2/Vs and I_{ON} of 4.4 μA. Additional observations can be found in **Tables S2** (SI). These results indicate that iptycene molecules located between the nanotubes and the oxide substrate have a relatively low impact on carrier mobility. It's worth noting that after further annealing at 300°C in vacuum, there is a noticeable decrease in carrier mobility, I_{ON}, and I_{ON}/I_{OFF} for both TG and BG configurations. This decrease is likely due to the decomposition of the iptycene alignment molecules that degraded the SWCNT device interfaces. To prevent such damage and deterioration, the devices should not be exposed to a temperature higher than 300 °C and for a period longer than 3 hours.

Furthermore, the best device was compared with 10 other CNTFETs created through the ART, fabricated and tested under the same conditions. The transport IV curves are shown in the SI, where the number of CNTs are indicated where possible. Of the 11 devices in total (**Figure 4**, **Table S3, Figures S3-S14**), quite large deviations were observed, though the devices were fabricated and tested under the same conditions. The I_{ON} ranged from 5.27 nA to 3.83 μA. The I_{ON}/I_{OFF} ratio varied from ~1E3 to ~1E6. The mobility was calculated to be in the range from 0.04 to 10.08 cm^2/Vs, with an average value of 1.44 cm^2/Vs. The large deviation for the I_{ON} could be attributed to the contact of the nanotube with the source and drain electrodes. Some of the nanotubes were wrapped by surfactant which increases dramatically the contact resistance. The added iptycene layer in contact with the tubes could also be a source of charge trapping and oxide effects, leading to the observed hysteresis in the V_G-I_{SD} plots and additional device-to-device variations.

Based on the IV characteristics in **Figure 2b**, the CNTFETs with ART do not form good ohmic contact with the electrodes but the performance is improved with annealing at 300°C. The contact junctions are evidenced by non-linear I-V characteristics near zero V_G bias and asymmetric conduction between positive and negative bias voltages, indicating the presence of Schottky barriers at the metal-CNT interfaces. The I-V curve becomes near linear at a higher V_G, where the transistor is at ON state, indicating that the Schottky barrier was overcome.

Overall, from the trends observed in **Figures 2** to **4**, the aligned top-gated devices showed improved FET performance and enhanced properties compared with the bundled devices. Currently, the performance of our aligned devices is limited by the lower packing density compared with state of art CNT transistors.[30, 31]

DFT calculations

To understand the interaction of the iptycene molecules with the CNTs, *ab initio* calculations within density functional theory (DFT) were conducted. We calculated the valence band maximum (VBM) and the conduction band minimum (CBM) levels of SWCNTs with the diameters close to the experimental one of 1 nm ((11,0), (8,4), (10,3), (13,0) and (10,5)). Then, the obtained values were compared with the highest occupied molecular orbital (HOMO) and the lowest occupied molecular orbital (LUMO) levels of the iptycene molecule and the precursor molecules from the synthesis of our iptycene such as Triptycene, 1,4-Dichloro-2-butene ($C_4H_6Cl_2$), 11,12-Bis(chloromethyl)-9,10-dihydro-9,10-ethanoanthracene ($C_{18}H_{16}Cl_2$), Bis(diethoxyphosphoryl) acetylene ($C_{10}H_{20}O_6P_2$) and 1,2,4,5-Tetrabromobenzene ($C_6H_2Br_4$), see **Figure S15** in SI.[27]

The energy diagram of HOMO/LUMO levels for individual semiconducting (10,3) SWCNTs with the iptycene relative to the vacuum level in comparison with VBM/CBM of SWCNT/Iptycene is presented in **Figure 5**. We found that in all the cases the VBM and CBM of SWCNTs lie in HOMO/LUMO gaps of molecules present in the system which indicates Type I alignment. In the meantime, the interaction of SWCNT with iptycene does not lead to the significant shift of VBM/CBM compared with the individual SWCNT (right panel "SWCNT + iptycene" in **Figure S15** in SI).

We analysed the electron density redistribution in the SWCNT/Iptycene interface area (see **Figure S16** in SI). At the interface, an electron loss for SWCNT was observed (cyan clouds) while the area closer to the iptycene molecule is characterized by an electron excess (yellow clouds). To compensate the electron loss, carbon atoms of the SWCNT located at the interface pull on the electron density from the SWCNT region located beyond the area of intersection, indicated by

yellow areas on the SWCNTs surface (bottom panel in **Figure S16** in SI). Based on bands alignment and charge redistribution in SWCNT/Iptycene hybrid system, the influence of the ART tweezer molecules to the electronic structure of SWCNT is negligible, which is consistent with experimental results of the similar carrier mobility measured from the TG and BG devices.

We calculated the binding energy between the iptycene and CNT via the equation: $E_b = E_{(total)} - E_{(molecule)} - E_{(CNT)}$, and the estimated values distributed from -1.15 eV to -1.43 eV per considered unit cell (or from -48.07 meV/carbon atom up to -55.01 meV/carbon atom), in dependence on the CNT diameter and chirality, which are correlate with our previous studies of van der Waals heterostructures.[32, 33] Due to the van der Waals nature of the interaction between a molecule and a nanotube, the contribution to the mechanical interaction in such structures is determined by the interaction area. We performed an estimation of the interaction between the iptycene and CNT surface. The values of the binding energy per surface area in molecule/CNT interface were varied from -9.33 meV/Å^2 up to -13.82 meV/Å^2. Effective surface area of interaction was determined as from 98.7 Å^2 up to 123.4 Å^2. These values correlate with the van der Waals interaction between the iptycene molecule and CNT.

Ammonia sensor

SWCNTs have been showcased in various sensory applications due to their entire surface atom structure.[34-37] Since monitoring of NH_3 is important for health, agricultural and environmental applications,[38-40] we investigated the potential of gas sensors with our aligned CNT device, used as a chemiresistor. The device was prepared and arranged as shown in **Figure S17a**, using commercially available semiconducting SWCNTs to demonstrate the versatility of the ART method.

The resistance of one bottom gated CNT transistor (**Figure S17b**) was measured under exposure to NH_3 at room temperature. The NH_3 vapor was introduced by passing a N_2 gas through a glass bottle of a 0.28% aqueous ammonia solution. The detailed experimental setup process is described in the SI, **Figure S18**. With only 2 ppm of NH_3, the current dropped 2.7 % within 100 s (**Figure S17c**). After switching the gas to pure N_2, the drop of current simultaneously ceased. By exposing the sensor again to the NH_3 gas again, the current dropped again, but with a smaller response (~1 %).

The sensitivity was calculated as follows: at 4 ppm of NH_3 gas the sensitivity was 0.49 ± 0.11 %/ppm for an exposure time of 60 seconds; at an exposure to 2 ppm NH_3 gas for 100 seconds, the sensitivity was 0.97 ± 0.21 %/ppm (**Table S4** and **S5** in SI). We speculate that the smaller response and slow recovery is due to the strong adsorption of NH_3 to SWCNTs surfaces.[41, 42] The error in standard deviation is due to partial irreversible adsorption, where the first response is higher as it occurs onto a fresh carbon nanotube surface which has a strong response to NH_3 that cannot be fully restored.[42] By omitting the first response in calculations for sensitivity, the values are 0.44 ± 0.04 %/ppm and 0.89 ± 0.13 %/ppm for the 4 ppm and 2 ppm gas exposures, respectively. Our data is comparable to that of reported ammonia sensors based on sc-SWCNT networks, such as reported by Cuniberti et al. that observed a sensitivity of 2.4%/ppm for long exposure (ca. 900 sec) to 2.5 ppm NH_3.[35]

Conclusions

As a proof of concept application, CNTFETs were fabricated with chirality-sorted (10,3) SWCNTs aligned by ART. Top-gated FETs demonstrated an I_{ON}/I_{OFF} of 2.9×10^6, carrier mobility of 10.08 cm^2/Vs, an I_{ON} of 3.8 µA, and a SS of 0.45 V/dec. Compared with the bundled network, the aligned CNTs show a 100x improvement on mobility, as the carriers can transport from source to drain

directly, rather than being impeded by the nanotube contacts. An NH_3 sensor based on aligned commercially available semiconducting SWCNTs showed a detection response to 2 and 4 ppm NH_3 exposure. The work shows the potential of uniformly aligned, chirality-sorted SWCNTs for their applications in FETs and gas sensors.

Experimental

Transistor fabrication

Single-walled carbon nanotubes were either 90% semiconducting purity in sodium dodecyl sulfate/sodium cholate (1%) aqueous buffer sourced from NanoIntegris Inc (Canada) or high purity (10,3) semiconducting SWCNTs separated from HiPco SWCNTs (NanoIntegris, Inc) by gel chromatography in a 0.5% sodium cholate aqueous solution. The average length of tubes was 0.73 um. The iptycenes were synthesized using previously established protocols.[23] A contact angle meter (CA-XP, Kyowa Interface Science) was used to evaluate the wettability of the silicon wafers after UV-ozone treatment and functionalization with an iptycene monolayer.

Bottom-gate (**Figure 1a**) and top-gate (**Figure 1c**) CNTFETs were fabricated using electron beam lithography (EBL). Top gates were constructed with a Cr/Pd/Au (1/10/50 nm) on a 20 nm atomic-layered deposited (ALD) Al_2O_3 insulating layer. Doped Si wafer was used as the back gate, with an oxide thickness of 200 nm. The devices were annealed at 300°C under argon for 3 hours to improve contact between SWCNT and substrate. An Elionix ELS-7500 DEX electron beam writer was employed with an electron acceleration of 50 kV and a beam current of 600 pA. A 575 μC/cm^2 electron irradiation dosage at 0.95 μs was applied to deposit large electrodes. The smaller electrodes that were in direct contact with the SWCNTs used a 600 μC/cm^2 electron irradiation amount at 1 μs. The single pixel size was 10 nm x 10 nm (x,y).

The patterning resist material was 950 PMMA-A4 (MicroChem Corp.) and the top conductive layer used Espacer-300Z (Showa Denko K.K). Samples were spin-coated at 2000 RPM and baked at 180°C for 3 minutes with the 950 PMMA-A4. The Espacer 300Z was deposited on the top after baking the PMMA, then the sample was once again subjected to spin-coating at 2000 RPM. No

further baking followed. Sample was then dipped in MilliQ H_2O for 10-15 s to remove the Espacer 300Z. Then, the PMMA layer was eliminated in a 3:1 solution of methyl isobutyl ketone (MIBK): isopropyl alcohol (IPA) for 45 seconds then washed immediately with IPA for 30 seconds and dried up under N_2 gas. An e-beam heating vacuum evaporator by ULVAC, Inc. was used to deposit the metals at 1 nm Cr/10 nm Pd/50 nm Au on the samples. The lift-off process used ZDMAC N,N-Dimethylacetamide liquid, followed by an IPA rinse to attain the EBL CNTFET devices.

The dielectric layer of 20 nm Al_2O_3 was deposited with Atomic Layer Deposition (ALD, SUNALER-R-150 ALS, Picosun). The layer was deposited via 170 cycles of alternating trimethylaluminum (TMA) and H_2O at 200°C. Thickness of the deposited alumina was verified with spectroscopic ellipsometry (DekTak 6M, Bruker) to be 20.9 nm on an individual Si (100) sample treated simultaneously with the fabricated devices. An Eiko multi-pocket e-beam evaporator was used to place the metals on the surface.

Electrical testing and analysis

The CNTFETs were analyzed using a Keithley 2636B source meter connected to an Agilent 4284A and an Appoloware M20 micro positioner. The CNTs connecting the source (S) and drain (D) electrodes were first detected using HR-SEM. Vacuum conditions were made possible with a Semi-auto Agilent 4156C measurement system at 22°C with a chamber pressure of approximately 10^{-3} Pa. The back gates were made via scratching the top of the wafers or employing conductive Ag paste on the sides of the substrate adhered to a Cu platform. The carrier mobility was extracted using the following equation:[43]

$$\mu = \frac{L_{SD}{}^2 G_m}{C V_{SD}} [\mathrm{cm^2/Vs}] \qquad \textbf{Equation 1}$$

Where $\boldsymbol{\mu}$ is the carrier mobility, $\mathbf{L_{SD}}$ is the gap length from the source and drain, $\mathbf{G_m}$ is the transconductance, **C** is the capacitance and $\mathbf{V_{SD}}$ is the bias from source to drain electrodes.

DFT calculations

Quantum chemical calculations were carried out using the density functional theory (DFT) [44, 45] implemented in Vienna Ab initio Simulation Package (VASP) program.[46-48] The exchange-correlation functional was calculated through generalized gradient approximation (GGA) in Perdew-Burke-Ernzerhof (PBE) parameterization[49] within the projector-augmented wave (PAW)[50] basis set technique was used. The energy cutoff of plane waves was set to be equal 400 eV. The first Brillouin zone was sampled according to Monkhorst-Pack scheme.[51] The atomic structure relaxation was carried out until the maximum value of interatomic forces became less than 0.05 eV/Å, and the energy variation between two steps of electronic loop became less than 10^{-5} eV. A vacuum region of at least 10 Å was chosen to avoid an artificial interaction between structures in non-periodic directions. To take into account van der Waals interactions we applied the Grimme correction (DFT-D3).[52]

Acknowledgements & funding

The authors acknowledge the assistance of Namiki Foundry NIMS for performing the EBL patterning and metal deposition. We thank Dr. Michio Matsumoto for assistance with the NMR and flash chromatography. The authors declare no competing financial interest. M.R.S acknowledges the International Cooperative Graduate Program from the National Institute for Materials Science for financial support. D.M.T. discloses support by JSPS Kakenhi projects (Grant No. JP20K05281, JP25820336, JP23H01796), JST-FOREST Program (grant number JPMJFR223T, Japan), WPI-MANA “Challenging Research Program (CRP)”, NIMS “Support system for curiosity-driven research”, and "Advanced Research Infrastructure for Materials and

Nanotechnology in Japan (ARIM)" of the Ministry of Education, Culture, Sports, Science and Technology (MEXT). Proposal Number JPMXP1224NM5238. E.V.S., Z.I.P., D.G.K. are grateful to the Joint Supercomputer Center of the Russian Academy of Sciences and to the Information Technology Centre of Novosibirsk State University for providing access to the cluster computational resources. D.J.S acknowledges the Natural Sciences and Engineering Research Council. T.T. and H.K. thank the support by JSPS KAKENHI Grants 20H05668 and 24K01282.

Author contributions

M.R.S performed the experiments and analyzed the data. M.R.S and D.M.T. wrote the manuscript. D.M.T. and D.J.S. supervised the project. S.I. evaluated the sensing properties. R. L. F. L. and M. F. G. calculated the gas sensitivity. N.L., T.T. (Takaaki Taniguchi) and S.L. assisted in the photolithography fabrication. K.T. assisted with device fabrication. T.T. (Takeshi Tanaka) and H.K. provided the sorted (10,3) SWCNTs. E.V.S., Z.I.P., and D.G.K. performed the DFT calculations. All authors commented and revised the manuscript.

Electronic Supplemental Material:

Equations of transport properties, fabrication parameters for metal deposition, calculations of density and alignment, additional I-V curves, electrical properties of iptycenes monolayer, sensing result and equipment setup.

Figures

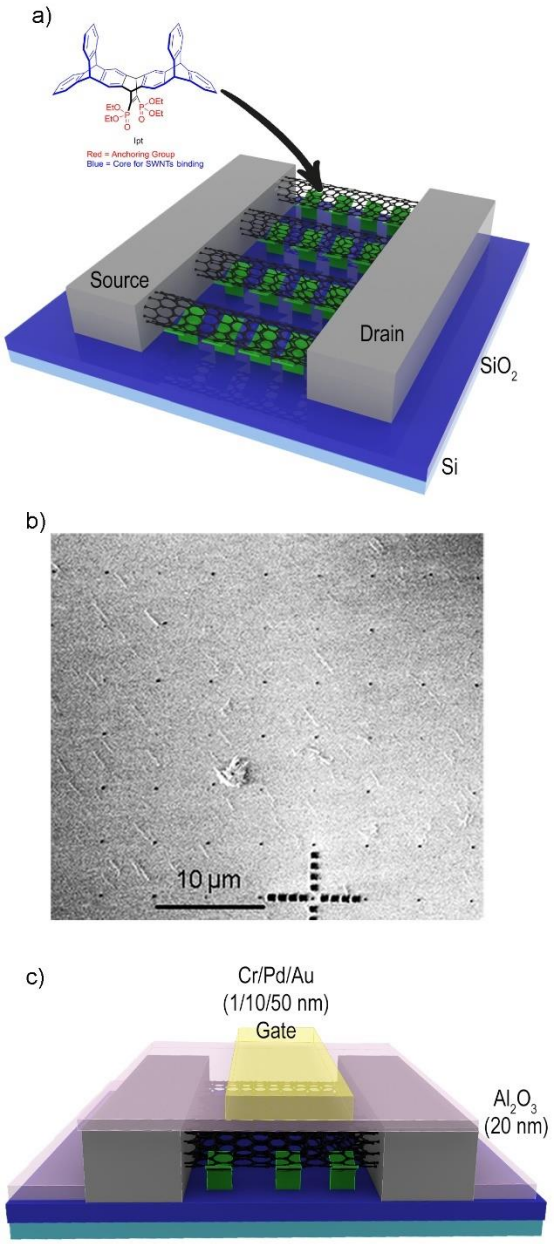

Figure 1. Alignment process and configuration of the device. a) Schematics of ART iptycene molecule on the bottom-gated device configuration, b) SEM image of ART aligned (10,3) SWCNTs on the silicon surface with gold dot and square markings, c) schematic of a top-gated CNTFET.

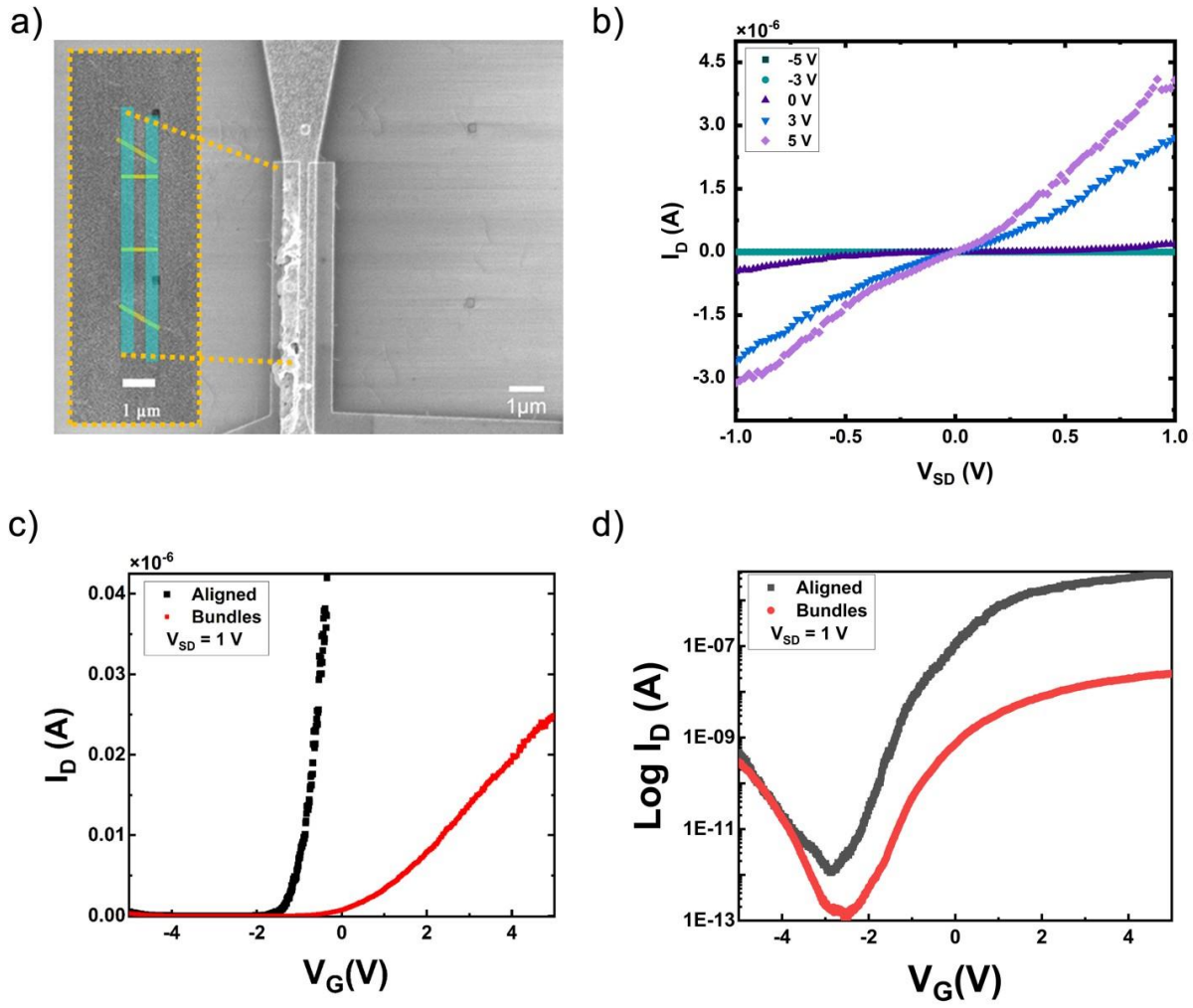

Figure 2. Characterization data of top gated (10,3) ART CNTFET. a) Scanning electron microscopy image of the carbon nanotube top-gated transistor with 4 aligned CNTs, b) Ids–Vds output curves and c-d) Ids–Vgs transport plots.

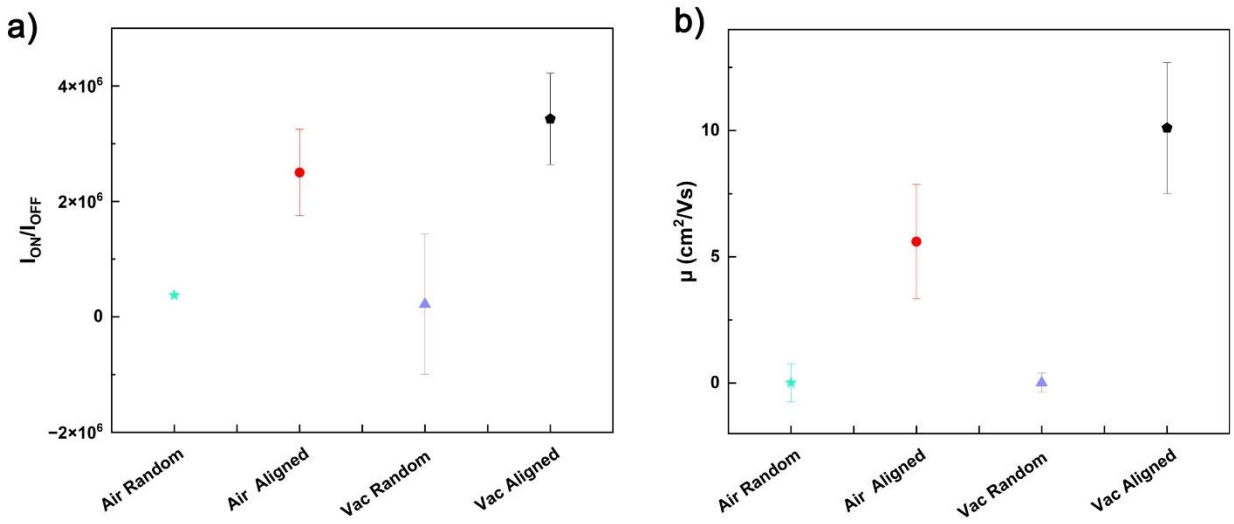

Figure 3. Statistical analysis and comparison of devices performance. Performance device comparisons for the top-gate configuration for the (10,3) SWCNTs bundles versus aligned SWCNTs for a) I_{ON}/I_{OFF} ratio and b) carrier mobility with standard deviations.

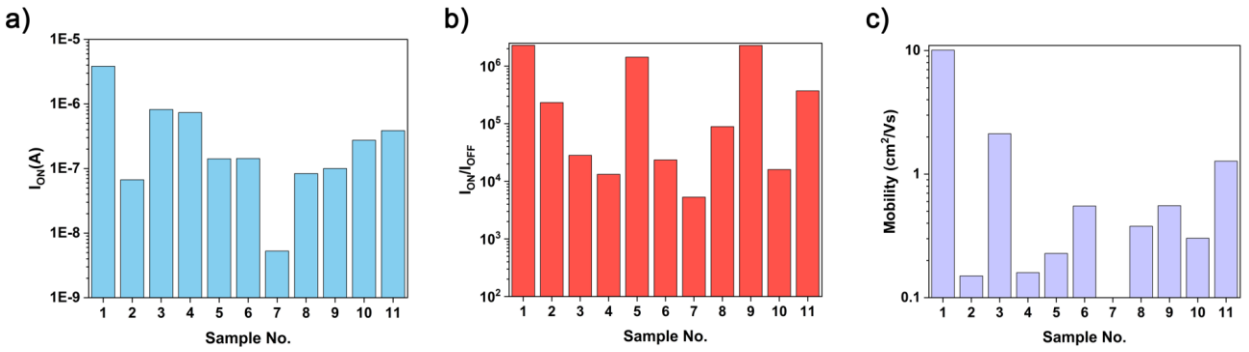

Figure 4. Histograms of I_{ON}, I_{ON}/I_{OFF} ratio and mobility of 11 devices a)I_{ON} b) I_{ON}/I_{OFF} ratio and c) mobility.

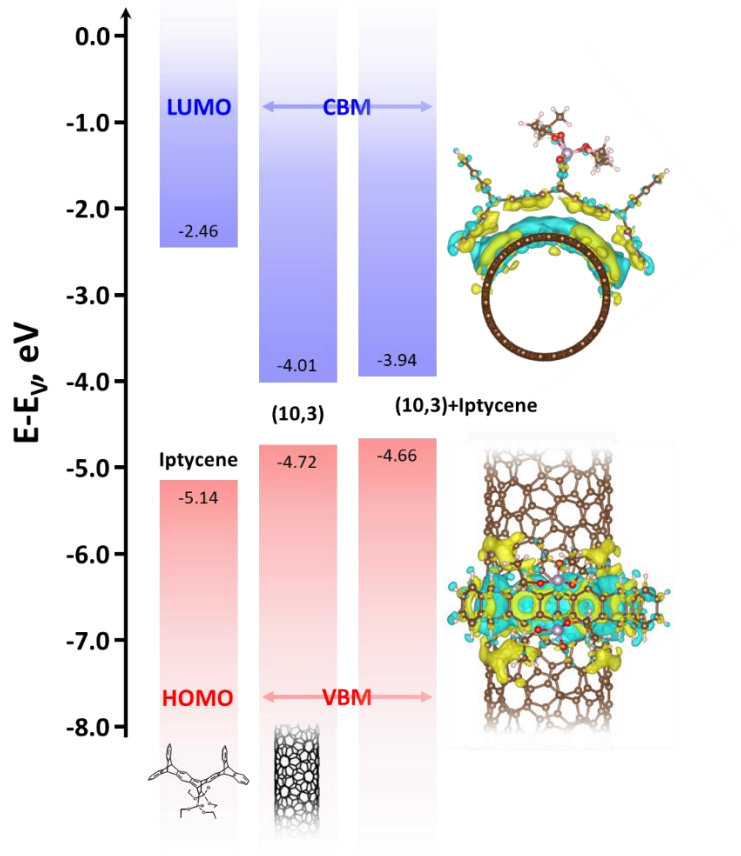

Figure 5. Electronic structure of Iptycene-CNT hybrid system. Energy diagram of HOMO/LUMO levels for individual semiconducting (10,3) SWCNT with the iptycene molecule relative to the vacuum level in comparison with VBM/CBM of SWCNT/Iptycene. Charge redistribution between the (10,3) SWCNT and Iptycene, is marked by yellow and blue cyan for electron accumulation and loss, respectively. The iso-surface level is 10^{-4} *e*/Å^3.

TOC

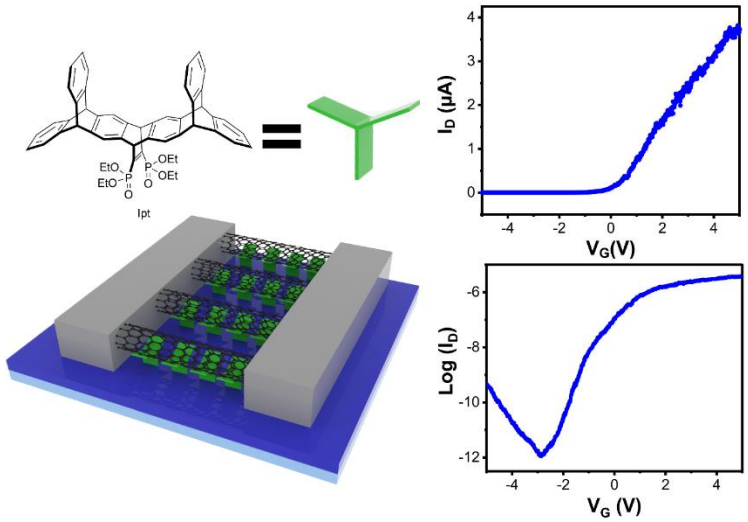

References

(1) Franklin, A. D. The road to carbon nanotube transistors. *Nature* **2013**, *498* (7455), 443-444. DOI: 10.1038/498443a
(2) Tang, D.-M.; Cretu, O.; Ishihara, S.; Zheng, Y.; Otsuka, K.; Xiang, R.; Maruyama, S.; Cheng, H.-M.; Liu, C.; Golberg, D. Chirality engineering for carbon nanotube electronics. *Nature Reviews Electrical Engineering* **2024**, *1* (3), 149-162. DOI: 10.1038/s44287-023-00011-8
(3) Franklin, A. D. Nanomaterials in transistors: From high-performance to thin-film applications. *Science* **2015**, *349* (6249), aab2750. DOI: 10.1126/science.aab2750
(4) Ghosh, S.; Bachilo, S. M.; Weisman, R. B. Advanced sorting of single-walled carbon nanotubes by nonlinear density-gradient ultracentrifugation. *Nature Nanotechnology* **2010**, *5*, 443, Article. DOI: 10.1038/nnano.2010.68
(5) Subbaiyan, N. K.; Cambré, S.; Parra-Vasquez, A. N. G.; Hároz, E. H.; Doorn, S. K.; Duque, J. G. Role of Surfactants and Salt in Aqueous Two-Phase Separation of Carbon Nanotubes toward Simple Chirality Isolation. *ACS Nano* **2014**, *8* (2), 1619-1628. DOI: 10.1021/nn405934y
(6) Cui, J.; Su, W.; Yang, D.; Li, S.; Wei, X.; Zhou, N.; Zhou, W.; Xie, S.; Kataura, H.; Liu, H. Mass Production of High-Purity Semiconducting Carbon Nanotubes by Hydrochloric Acid Assisted Gel Chromatography. *ACS Applied Nano Materials* **2019**, *2* (1), 343-350. DOI: 10.1021/acsanm.8b01942
(7) Liu, H.; Nishide, D.; Tanaka, T.; Kataura, H. Large-scale single-chirality separation of single-wall carbon nanotubes by simple gel chromatography. *Nat Commun* **2011**, *2* (1), 309. DOI: 10.1038/ncomms1313
(8) Liu, H.; Tanaka, T.; Urabe, Y.; Kataura, H. High-Efficiency Single-Chirality Separation of Carbon Nanotubes Using Temperature-Controlled Gel Chromatography. *Nano Lett* **2013**, *13* (5), 1996-2003. DOI: 10.1021/nl400128m
(9) Wang, G.; Wei, X.; Tanaka, T.; Kataura, H. Diameter-Selective Separation of Semiconducting Single-Walled Carbon Nanotubes in Large Diameter Range. *physica status solidi (b)* **2017**, *254* (11), 1700294. DOI: 10.1002/pssb.201700294
(10) Yahya, I.; Bonaccorso, F.; Clowes, S. K.; Ferrari, A. C.; Silva, S. R. P. Temperature dependent separation of metallic and semiconducting carbon nanotubes using gel agarose chromatography. *Carbon* **2015**, *93*, 574-594. DOI: 10.1016/j.carbon.2015.05.036
(11) Ajayan, P. M.; Stephan, O.; Colliex, C.; Trauth, D. Aligned carbon nanotube arrays formed by cutting a polymer resin-nanotube composite. *Science* **1994**, *265*, 1212+, Article. (acccessed 2020/5/14/). From Gale Gale Academic OneFile.
(12) Krupke, R.; Hennrich, F.; Löhneysen, H. v.; Kappes, M. M. Separation of Metallic from Semiconducting Single-Walled Carbon Nanotubes. *Science* **2003**, *301* (5631), 344-347. DOI: doi:10.1126/science.1086534
(13) Liu, H.; Tanaka, T.; Kataura, H. Optical Isomer Separation of Single-Chirality Carbon Nanotubes Using Gel Column Chromatography. *Nano Letters* **2014**, *14* (11), 6237-6243. DOI: 10.1021/nl5025613
(14) Xiao, Z.; Elike, J.; Reynolds, A.; Moten, R.; Zhao, X. The fabrication of carbon nanotube electronic circuits with dielectrophoresis. *Microelectronic Engineering* **2016**, *164*, 123-127. DOI: https://doi.org/10.1016/j.mee.2016.07.013
(15) Lutz, T.; Donovan, K. J. Macroscopic scale separation of metallic and semiconducting nanotubes by dielectrophoresis. *Carbon* **2005**, *43* (12), 2508-2513. DOI: https://doi.org/10.1016/j.carbon.2005.05.002
(16) Arnold, M. S.; Green, A. A.; Hulvat, J. F.; Stupp, S. I.; Hersam, M. C. Sorting carbon nanotubes by electronic structure using density differentiation. *Nature Nanotechnology* **2006**, *1* (1), 60-65. DOI: 10.1038/nnano.2006.52
(17) Ma, Y.; Wang, B.; Wu, Y.; Huang, Y.; Chen, Y. The production of horizontally aligned single-walled carbon nanotubes. *Carbon* **2011**, *49* (13), 4098-4110. DOI: https://doi.org/10.1016/j.carbon.2011.06.068

(18) Fujii, S.; Tanaka, T.; Nishiyama, S.; Kataura, H. High performance thin-film transistors using moderately aligned semiconducting single-wall carbon nanotubes. *physica status solidi (b)* **2011**, *248* (11), 2692-2696, https://doi.org/10.1002/pssb.201100254
(19) Tulevski, G. S.; Hannon, J.; Afzali, A.; Chen, Z.; Avouris, P.; Kagan, C. R. Chemically Assisted Directed Assembly of Carbon Nanotubes for the Fabrication of Large-Scale Device Arrays. *Journal of the American Chemical Society* **2007**, *129* (39), 11964-11968. DOI: 10.1021/ja073647t
(20) Sharma, R.; Strano, M. S. Centerline Placement and Alignment of Anisotropic Nanotubes in High Aspect Ratio Cylindrical Droplets of Nanometer Diameter. *Advanced Materials* **2009**, *21* (1), 60-65. DOI: https://doi.org/10.1002/adma.200801287
(21) Qiu, S.; Wu, K.; Gao, B.; Li, L.; Jin, H.; Li, Q. Solution-Processing of High-Purity Semiconducting Single-Walled Carbon Nanotubes for Electronics Devices. *Advanced Materials* **2019**, *31* (9), 1800750. DOI: https://doi.org/10.1002/adma.201800750
(22) Su, W.; Yang, D.; Cui, J.; Wang, F.; Wei, X.; Zhou, W.; Kataura, H.; Xie, S.; Liu, H. Ultrafast wafer-scale assembly of uniform and highly dense semiconducting carbon nanotube films for optoelectronics. *Carbon* **2020**, *163*, 370-378. DOI: https://doi.org/10.1016/j.carbon.2020.03.032
(23) Snowdon, M. Introduction. In *Methods of the Alignment-Relay Technique for Nanosystems: Optimization and Innovation*, Snowdon, M. Ed.; Springer International Publishing, 2021; pp 1-63.
(24) Kulak, M. R.; Schipper, D. J. Carbon nanotube alignment and sorting: Attempting a sulfur moiety as anchoring component. *Phosphorus, Sulfur, and Silicon and the Related Elements* **2019**, *194* (7), 760-763. DOI: 10.1080/10426507.2019.1603234
(25) Yomogida, Y.; Tanaka, T.; Zhang, M.; Yudasaka, M.; Wei, X.; Kataura, H. Industrial-scale separation of high-purity single-chirality single-wall carbon nanotubes for biological imaging. *Nature Communications* **2016**, *7* (1), 12056. DOI: 10.1038/ncomms12056
(26) Snowdon, M. R.; Wang, S.; Mashmoushi, N.; Hopkins, S. W.; Schipper, D. J. Carboxylic acids as anchoring components on aluminum oxide for the alignment relay technique of single-walled carbon nanotubes. *New Journal of Chemistry* **2021**, *45* (12), 5340-5349, 10.1039/D0NJ05154C. DOI: 10.1039/D0NJ05154C
(27) Snowdon, M.; Selmani, S.; Schipper, D. J. Sonication-Enhanced Alignment Relay Technique for the Orientation of Single-Walled Carbon Nanotubes. *ACS Applied Nano Materials* **2019**, *2* (10), 6637-6645. DOI: 10.1021/acsanm.9b01514
(28) Snowdon, M. Modifications to the ART Procedure. In *Methods of the Alignment-Relay Technique for Nanosystems: Optimization and Innovation*, Springer International Publishing, 2021; pp 65-99.
(29) Collins, P. G.; Bradley, K.; Ishigami, M.; Zettl, A. Extreme Oxygen Sensitivity of Electronic Properties of Carbon Nanotubes. *Science* **2000**, *287* (5459), 1801-1804. DOI: doi:10.1126/science.287.5459.1801
(30) Qiu, C.; Zhang, Z.; Xiao, M.; Yang, Y.; Zhong, D.; Peng, L.-M. Scaling carbon nanotube complementary transistors to 5-nm gate lengths. *Science* **2017**, *355* (6322), 271. DOI: 10.1126/science.aaj1628
(31) Liu, L.; Han, J.; Xu, L.; Zhou, J.; Zhao, C.; Ding, S.; Shi, H.; Xiao, M.; Ding, L.; Ma, Z.; et al. Aligned, high-density semiconducting carbon nanotube arrays for high-performance electronics. *Science* **2020**, *368* (6493), 850. DOI: 10.1126/science.aba5980
(32) Kvashnin, D. G.; Baidyshev, V. S. Study of formation and properties of F4TCNQ/MoS2 heterostructures with point defects driven by DFT and neural network potential. *FlatChem* **2023**, *42*, 100585. DOI: https://doi.org/10.1016/j.flatc.2023.100585
(33) Sukhanova, E. V.; Popov, Z. I.; Kvashnin, D. G. Theoretical Study of the Electronic and Optical Properties of a Heterostructure Based on PTCDA Organic Semiconductor and MoSe2. *JETP Letters* **2020**, *111* (11), 627-632. DOI: 10.1134/S0021364020110090
(34) Ishihara, S.; Bahuguna, A.; Kumar, S.; Krishnan, V.; Labuta, J.; Nakanishi, T.; Tanaka, T.; Kataura, H.; Kon, Y.; Hong, D. Cascade reaction-based chemiresistive array for ethylene sensing. *ACS Sensors* **2020**, *5* (5), 1405-1410. DOI: 10.1021/acssensors.0c00194

(35) Panes-Ruiz, L. A.; Shaygan, M.; Fu, Y.; Liu, Y.; Khavrus, V.; Oswald, S.; Gemming, T.; Baraban, L.; Bezugly, V.; Cuniberti, G. Toward Highly Sensitive and Energy Efficient Ammonia Gas Detection with Modified Single-Walled Carbon Nanotubes at Room Temperature. *ACS Sensors* **2018**, *3* (1), 79-86. DOI: 10.1021/acssensors.7b00358
(36) Freddi, S.; Emelianov, A. V.; Bobrinetskiy, I. I.; Drera, G.; Pagliara, S.; Kopylova, D. S.; Chiesa, M.; Santini, G.; Mores, N.; Moscato, U.; et al. Development of a Sensing Array for Human Breath Analysis Based on SWCNT Layers Functionalized with Semiconductor Organic Molecules. *Advanced Healthcare Materials* **2020**, *9* (12), 2000377. DOI: https://doi.org/10.1002/adhm.202000377
(37) Ishihara, S. Portable Toxic Gas Sensors Based on Functionalized Carbon Nanotubes. In *System-Materials Nanoarchitectonics*, Wakayama, Y., Ariga, K. Eds.; Springer Japan, 2022; pp 161-167.
(38) Snow, E. S.; Perkins, F. K.; Robinson, J. A. Chemical vapor detection using single-walled carbon nanotubes. *Chem Soc Rev* **2006**, *35* (9), 790-798. DOI: 10.1039/b515473c
(39) Kauffman, D. R.; Star, A. Carbon Nanotube Gas and Vapor Sensors. *Angewandte Chemie International Edition* **2008**, *47* (35), 6550-6570. DOI: https://doi.org/10.1002/anie.200704488
(40) Schroeder, V.; Savagatrup, S.; He, M.; Lin, S.; Swager, T. M. Carbon Nanotube Chemical Sensors. *Chemical Reviews* **2019**, *119* (1), 599-663. DOI: 10.1021/acs.chemrev.8b00340
(41) Abbas, S.; Yi, W.; Yoo, S.; Khalid, A.; Bhalli, Z.; Si, J.; Hou, X. Highly Efficient Response of Ammonia Gas Sensor Based on Surfactant-Free Sorted-Semiconducting Single-Walled Carbon Nanotubes at Room Temperature. *physica status solidi (a)* **2022**, *219* (7), 2100529. DOI: https://doi.org/10.1002/pssa.202100529
(42) Lee, C. Y.; Strano, M. S. Understanding the Dynamics of Signal Transduction for Adsorption of Gases and Vapors on Carbon Nanotube Sensors. *Langmuir* **2005**, *21* (11), 5192-5196. DOI: 10.1021/la046867i
(43) Trivedi, K.; Yuk, H.; Floresca, H. C.; Kim, M. J.; Hu, W. Quantum Confinement Induced Performance Enhancement in Sub-5-nm Lithographic Si Nanowire Transistors. *Nano Lett* **2011**, *11* (4), 1412-1417. DOI: 10.1021/nl103278a
(44) Hohenberg, P.; Kohn, W. Inhomogeneous Electron Gas. *Physical Review* **1964**, *136* (3B), B864-B871. DOI: 10.1103/PhysRev.136.B864
(45) Kohn, W.; Sham, L. J. Self-consistent equations including exchange and correlation effects. *Physical review* **1965**, *140* (4A), A1133
(46) Kresse, G.; Furthmüller, J. Efficient iterative schemes for ab initio total-energy calculations using a plane-wave basis set. *Physical review B* **1996**, *54* (16), 11169
(47) Kresse, G.; Furthmüller, J. Efficiency of ab-initio total energy calculations for metals and semiconductors using a plane-wave basis set. *Computational materials science* **1996**, *6* (1), 15-50.
(48) Kresse, G.; Hafner, J. Ab initio molecular-dynamics simulation of the liquid-metal--amorphous-semiconductor transition in germanium. *Physical Review B* **1994**, *49* (20), 14251-14269. DOI: 10.1103/PhysRevB.49.14251
(49) Perdew, J. P.; Burke, K.; Ernzerhof, M. Generalized Gradient Approximation Made Simple. *Physical Review Letters* **1996**, *77* (18), 3865-3868. DOI: 10.1103/PhysRevLett.77.3865.
(50) Blöchl, P. E. Projector augmented-wave method. *Physical Review B* **1994**, *50* (24), 17953-17979. DOI: 10.1103/PhysRevB.50.17953
(51) Monkhorst, H. J.; Pack, J. D. Special points for Brillouin-zone integrations. *Physical Review B* **1976**, *13* (12), 5188-5192. DOI: 10.1103/PhysRevB.13.5188
(52) Grimme, S.; Antony, J.; Ehrlich, S.; Krieg, H. A consistent and accurate ab initio parametrization of density functional dispersion correction (DFT-D) for the 94 elements H-Pu. *The Journal of Chemical Physics* **2010**, *132* (15), 154104. DOI: 10.1063/1.3382344